Hindawi
Adsorption Science & Technology
Volume 2022, Article ID 5455330, 18 pages
https://doi.org/10.1155/2022/5455330

Research Article

Adsorption Properties of Modified ATP-RGO Composite Aerogel for Removal of Malachite Green and Methyl Orange from Unitary and Binary Aqueous Solutions

Hong Ji Li, Jia Hui Xu, Liu Qing Wang, Dan Dan Hou, Zhi Ru Wang, and Hao Zhuo Li

School of Urban Planning and Municipal Engineering Xi'an Polytechnic University, Xi'an 710048, China

Correspondence should be addressed to Hong Ji Li; lhj861106@126.com

Received 23 May 2022; Revised 24 June 2022; Accepted 19 July 2022; Published 2 August 2022

Academic Editor: Hesham Hamad

In this paper, the modified attapulgite-reduced graphene oxide composite aerogel (ATP-RGO CA) was prepared by sol-gel method using modified attapulgite as silica source. The removal of the cationic dye malachite green (MG) and azo dye methyl orange (MO) onto ATP-RGO CA from unitary and binary systems was investigated. Morphology and microstructure studies of ATP-RGO CA were investigated by Fourier transform infrared (FTIR), scanning electron microscopy (SEM), X-ray diffraction (XRD), and specific surface area and porosity analysis. Experiments were carried out as a function of pH, contact time, initial dye concentration, and temperature in unitary and binary systems. The adsorption kinetics, isotherms, thermodynamics, and dye desorption were studied in unitary and binary dye systems. The adsorption kinetics was modeled using the pseudo-first-order, pseudo-second-order, and intraparticle diffusion kinetics equations. The equilibrium adsorption data of MG and MO dyes on ATP-RGO CA were analyzed. Thermodynamic parameters of dye adsorption were obtained. In addition, the regeneration of ATP-RGO CA was studied using dye desorption in unitary and binary dye systems. The adsorption kinetics of the dyes followed pseudo-second-order kinetics. The results indicate that the Langmuir model provides the best correlation of the experimental data. The thermodynamic studies showed that the dye adsorption onto ATP-RGO CA was a spontaneous and endothermic reaction. High desorption of MG and MO showed the regeneration of ATP-RGO CA. It can be concluded that ATP-RGO CA is suitable as an adsorbent material to remove MG and MO dyes from unitary and binary systems.

1. Introduction

Dyes are widely used in various industries including textile, cosmetics, paper, plastics, rubber, and coating. Their discharge into water causes serious environmental and health problems [1]. Most of these dyes contain aromatic rings, which make them carcinogenic and mutagenic. Dyes can cause allergy, dermatitis, and skin irritation and also provoke cancer and mutation in humans [2]. At the same time, their complex molecular structure makes them very stable and difficult for biodegradation [3]. Therefore, the removal of color from waste effluents has become environmentally important. Many researchers have made considerable attempts to find suitable treatment systems to treat wastewater containing dyes from different industries, especially the textile industry.

Cationic dye malachite green (MG) and azo dye methyl orange (MO) are the representatives of dyes. MG and MO dyes have a negative impact on human health and increase the risk of cancer. Those used in the food industry are related to the appearance of allergy, asthma, dermatitis, and vascular edema [4], while the use in the pharmaceutical industry is alleged to cause skin irritation. MG rapidly metabolizes into fat-soluble colorless malachite green when it enters aquatic animals. MG has potential carcinogenic, teratogenic, and mutagenic effects. The wastewater formed by MO contains –N=N– components that are difficult to degrade, and carcinogens will be produced under certain

conditions. MG and MO dyes are toxic due to the presence of aromatic rings in their structures. Dye degradation is not easy and can induce the following diseases: dizziness, jaundice, burns, allergic problems, vomiting, diarrhea, nausea, and even affect development and mental health [4]. Due to the stable chemical properties and obvious toxicity of MG and MO, it is considered as a refractory organic wastewater by researchers [5]. The commonly used methods for dye removal from waste effluents are adsorption [6], coagulation [7, 8], biodegradation [9], membrane process, etc. [10, 11]. At present, the most common technique is adsorption technology, which is popular for its effectiveness, efficiency, economy, and absence of secondary pollution [12].

Recent studies have also confirmed that adsorption is a reliable and effective method for removing dyes from dye wastewater. Li et al. [13] prepared polyvinyl alcohol/graphene oxide adsorption sponge by crosslinking graphene oxide and polyvinyl alcohol. The adsorption sponge has ultralow density, good mechanical properties, and excellent continuous flow adsorption capacity. Sobhanardakani et al. [14] studied the adsorption of malachite green (MG), Nile blue A (NB), and Janus green B (JG) dyes on $NiFe_2O_4$ nanoparticles. Wu et al. [15] used ethyl silicate as the precursor, anhydrous ethanol as solvent, and γ-methacryloxypropyltrimethoxysilane as a modifier to prepare hydrophobic SiO_2 aerogel by sol-gel two-step catalytic method. The results show that the temperature resistance can reach 407°C, the specific surface area is 877.17 $m^2 \cdot g^{-1}$, the pore size distribution is 1.9~5 nm, and the particle size range is 10~50 nm. It is a typical nano-mesoporous material. These studies have shown that adsorption has a good effect on the removal of dyes from aqueous solutions, but few researchers pay attention to the cost and mechanical strength of the prepared adsorbents. Due to the use of expensive raw materials, the prepared adsorbents are unacceptable under large-scale production conditions. Moreover, if the mechanical strength of the adsorbent is not ideal, the potential cost generated in production activities is also immeasurable. Therefore, it is very important for researchers to find economical raw materials and prepare adsorbents with high mechanical strength and excellent adsorption performance to remove dyes from dye-polluted wastewater [16, 17].

In this manuscript, we used cheap natural attapulgite modified as silicon source to extract amorphous silicon oxides. The modified attapulgite-reduced graphene oxide composite aerogel (ATP-RGO CA) was synthesized by the sol-gel method. We report a detailed application of ATP-RGO CA as an adsorbent for the removal of dyes: methyl orange (MO) and malachite green (MG). The morphology features of ATP-RGO CA were characterized by Fourier transform infrared (FTIR), scanning electron microscopy (SEM), X-ray diffraction (XRD), and specific surface area and porosity analysis. The impact of external adsorption conditions such as pH value, contact time, and adsorption temperature on the adsorption process of unitary and binary dye systems was successfully achieved. To achieve the adsorption capacity and mechanisms of MG and MO adsorption onto ATP-RGO CA, the equilibrium kinetic, isotherm, and thermodynamic parameters were studied. The reusability test of ATP-RGO CA was performed by carrying out five cycles of adsorption-desorption studies. This study provides a useful reference for the preparation and application evaluation of dye adsorbents in the future.

2. Materials and Methods

2.1. Chemicals and Materials. Graphite powder, concentrated sulfuric acid, potassium permanganate, hydrochloric acid, and sodium nitrate are analytical pure, purchased from Tianjin Tianli Chemical Reagent Co., Ltd.; hydrogen peroxide, purchased from Tianjin Damao chemical reagent factory; ascorbic acid, concentration for analysis pure, purchased from Tianjin Tianxin Fine Chemical Development Center; malachite green, methyl orange, sodium hydroxide, sodium chloride, trimethylchlorosilane, and n-hexane are analytical pure, purchased from Tianjin Comiou Chemical reagent Co., Ltd. All the used chemicals are of analytical grade and without further purification. Attapulgite was collected from a real estate company in Gansu Province.

2.2. Preparation of Graphene Aerogel and Composite Aerogel

2.2.1. Preparation of Graphene Oxide. Add graphite powder and sodium nitrate at a ratio of 1 : 2 in 50 mL concentrated sulfuric acid and react for 40 min in the ice bath. Then, potassium permanganate was added in batches and fully reacted; heating, stirring at the same time, and then slowly dropping water, full reaction15 minutes, according to the water and ultrapure water volume ratio of 1 : 8 in the solution, after filtration. The filter cake was washed with dilute hydrochloric acid, dispersed with pure water, and centrifuged. The obtained graphene oxide sample was dried at 40°C [18].

2.2.2. Preparation of Graphene Aerogel. Graphene oxide solution of 4 mg·mL-1 was mixed uniformly by ultrasonic stirring. The graphene oxide and ascorbic acid were mixed according to the mass ratio of 1 : 2.5. The mixed solution after ultrasonic vibration treatment was put into a reaction kettle and heated in an oven at 90°C for 2 h to prepare the thermally reduced graphene hydrogel in the effluent [19]. Remove static to room temperature after multiple cleaning dialyzes in ethanol aqueous solution [20], after freeze-drying machine processing graphene aerogel.

2.2.3. Preparation of Modified ATP-RGO Composite Aerogel. Attapulgite was immersed in hydrochloric acid with a concentration of 9%. After shaking in a water bath shaker at 25°C and 30 rad/min for 30 min, it was moved to a water bath pot, stirred every 30 min at 70°C, cooled to room temperature after 8 h, and dried after filtration [21]. The 2.00 g acid-modified attapulgite was placed in a 50 mL small beaker, and hydrochloric acid with a concentration of 9% was added. The mixture was stirred evenly with a glass rod and moved to a hydrothermal crystallization reactor with polytetrafluoroethylene as the lining. The mixture was placed in an oven at 180°C and cooled to room temperature after 12 h. The mixture was filtered and dried with a circulating

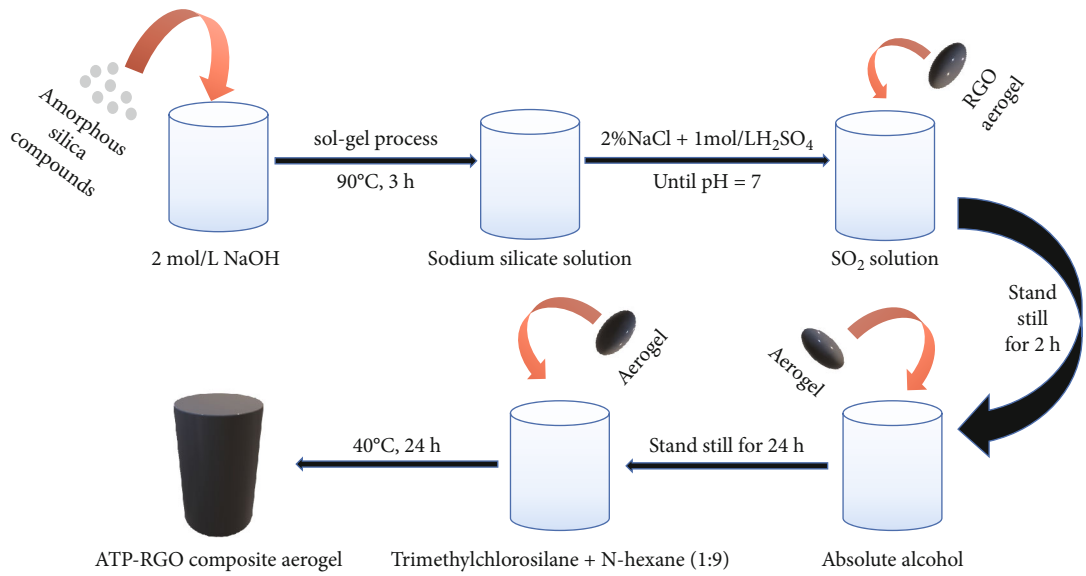

Figure 1: Preparation scheme of ATP-RGO composite aerogels.

vacuum pump to obtain a white powdered solid, which was the silicon source [22].

Add silicon source into 2 mol·L^{-1} NaOH solution reacted at 90°C for 3 hours, and the solution was filtered to remove insoluble residues. Sodium chloride solution with a mass fraction of 4% and saturated sodium silicate solution with the same volume were mixed at room temperature, and dilute sulfuric acid solution with a mass fraction of 1 mol·L^{-1} was added when stirring to form silica sol (pH = 7). Reduced graphene oxide (RGO) was impregnated in the sol and fully washed after solidification.

After standing for 2 h at room temperature, the water in the gel was washed and replaced with a 50% ethanol solution. After aging for 12 h at room temperature, the gel was further aged with anhydrous ethanol for 24 h. Trimethylchlorosilane and n-hexane were mixed evenly as modifiers according to the volume ratio of 1 : 9, and the sample was immersed in it for 24 h at 40°C for hydrophobic treatment. After modification, modified ATP-RGO composite aerogel was prepared by fully washing and drying with n-hexane. A brief preparation procedure of ATP-RGO composite aerogel is demonstrated in Figure 1.

2.3. Experimental Method

2.3.1. Adsorption Experiment. The concentration of 500 mg·L^{-1} MG, MO solution 100 mL, adding 20 mg composite aerogel, shaking the water bath at 25°C for 6 hours, sampling every other time, and determination of MG, MO absorbance. The removal rate and adsorption amount of MG and MO dye systems by composite aerogel were calculated. Experimental design adjusted pH to 2, 4, 6, 8, and 10; the initial dye concentration was 200 mg·L^{-1}, 300 mg·L^{-1}, 400 mg·L^{-1}, and 500 mg·L^{-1}. The set temperature is 25°C, 35°C, and 45°C three temperatures; Langmuir and Freundlich's isothermal adsorption models were used to fit the adsorption experimental results of composite aerogel. The effect of contact time on dye removal rate was investigated by selecting a certain time node as the contact time. The calculation formulas of MG and MO removal rate η and equilibrium adsorption capacity q_e are as follows:

$$\eta = \frac{\rho_0 - \rho_e}{\rho_0} \times 100\%, \tag{1}$$

$$q_e = \frac{(\rho_0 - \rho_e)V}{m}, \tag{2}$$

where ρ_0 and ρ_e are the dye concentration at the initial stage and equilibrium stage (mg/L), V is the volume of reaction solution (L), and m is the quality of adsorbent (g).

To better explain the adsorption mechanism in the adsorption process, several adsorption models were fitted in this study. Pseudo-first-order kinetic (Equation (3)), pseudo-second-order kinetic (Equation (4)), and intraparticle diffusion (Equation (5)) are three classical kinetic models that reveal the adsorption process. The equation is as follows:

$$\ln(q_e - q_t) = \ln q_e - k_1 t, \tag{3}$$

$$\frac{t}{q_t} = \frac{1}{k_2 q_e^2} + \frac{1}{q_e} t, \tag{4}$$

$$q_t = k_p\left(t^{1/2}\right), \tag{5}$$

where q_e and q_t are the adsorption capacity of composite aerogel at equilibrium and at different times (mg/g). k_1 (min^{-1}), k_2 (g·mg^{-1}·min^{-1}), and k_p (g·mg^{-1}·min$^{-1/2}$) are the kinetic rate constants. t (min) is the adsorption time.

Langmuir, Freundlich, and Temkin isothermal adsorption models are the three most commonly used adsorption models for wastewater treatment. Therefore, in this study, the Langmuir model (Equation (6)), Freundlich model

Table 1: L9 (34) orthogonal design and experimental results.

Serial number	Combination	A	B	C	Gelling time T (min)	Mechanical strength J (g)
1	$A_1B_1C_1$	1 : 10	25	40	10	93
2	$A_1B_2C_2$	1 : 10	40	60	7	83
3	$A_1B_3C_3$	1 : 10	55	80	3	97
4	$A_2B_1C_2$	1 : 15	25	60	8	85
5	$A_2B_2C_3$	1 : 15	40	80	9	91
6	$A_2B_3C_1$	1 : 15	55	40	4	100
7	$A_3B_1C_3$	1 : 20	25	80	5	92
8	$A_3B_2C_1$	1 : 20	40	40	15	90
9	$A_3B_3C_2$	1 : 20	55	60	6	95
T mean value 1	K_1	20	23	29		
T mean value 2	K_2	21	31	19		
T mean value 3	K_3	26	13	17		
T range	R_j	6	18	12		
J mean value 1	Q_1	263	270	283		
J mean value 2	Q_2	276	264	263		
J mean value 3	Q_3	277	292	280		
J range	R_j	14	28	20		

(Equation (7)), and Temkin model (Equation (8)) were used to fit the adsorption isotherms of MG and MO on composite aerogel. The equation is as follows:

$$\frac{C_e}{q_e} = \frac{1}{Q_{\max}k_L} + \frac{C_e}{Q_{\max}}, \tag{6}$$

$$\ln q_e = \ln k_F + \frac{\ln C_e}{n}, \tag{7}$$

$$q_e = k_T \ln (fC_e), \tag{8}$$

where C_e (mg·L^{-1}) is the equilibrium concentration. $Q_{\max}$ (mg·g^{-1}) is the theoretical maximum adsorption capacity of composite aerogel. k_L (L·mg^{-1}), k_F (mg·g^{-1}), and k_T (J/mol) are the constants of Langmuir, Freundlich, and Temkin isotherms. n represents the adsorption intensity, and f (L/mg) is the Temkin binding energy.

To further evaluate the adsorption process, one of the key parameters of the Langmuir equation R_L was calculated (Equation (9)); R_L is a dimensionless separation growth factor that examines whether the adsorption process is favorable.

$$R_L = \frac{1}{1 + K_L C_e}. \tag{9}$$

If $R_L > 1$, it indicates that the adsorption is not favorable; if $R_L = 1$, the adsorption is linear; if $0 < R_L < 1$, the adsorption is favorable, and if $R_L = 0$, it means that adsorption is irreversible [23].

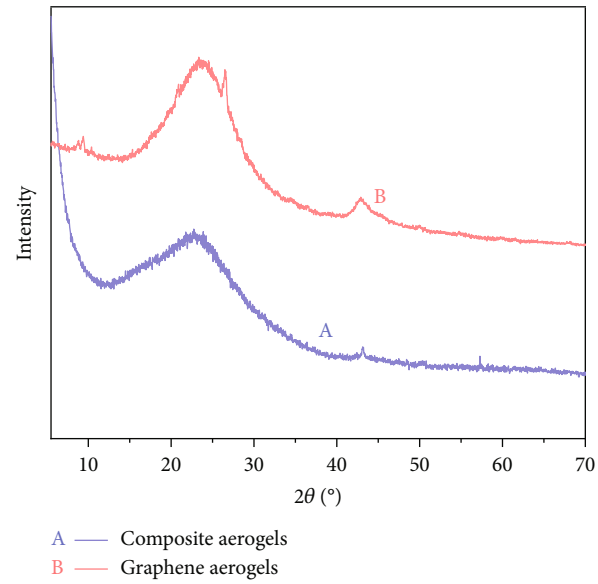

Figure 2: X-ray diffraction patterns of graphene aerogels and composite aerogels.

To study the dependency of the MG and MO adsorption process on the temperature, the equilibrium data were evaluated in terms of thermodynamics. The effects of different operating temperatures (298.15 K, 308.15 K, and 318.15 K) are investigated in this research. The thermodynamic parameters enthalpy (ΔH), entropy (ΔS), and free energy (ΔG) alteration were studied to the determination of the thermodynamic behavior of the adsorption process. The

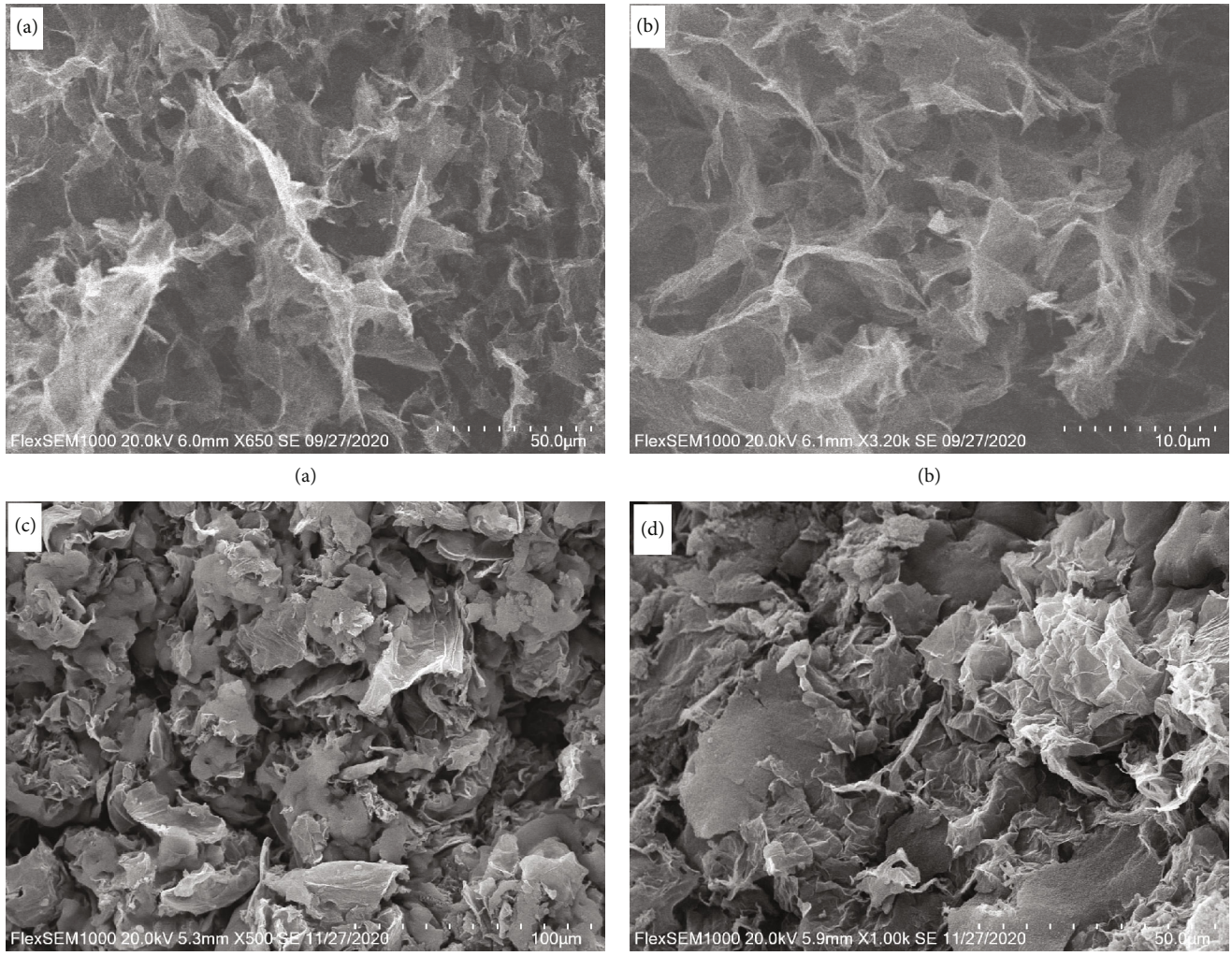

Figure 3: SEM of (a, b) graphene aerogel and (c, d) composite aerogel.

changes in the thermodynamic parameters were calculated with the following equation:

$$\Delta G^0 = -RT \ln k_d, \tag{10}$$

$$k_d = \frac{q_e}{c_e}, \tag{11}$$

$$\ln k_d = \frac{\Delta S}{R} - \frac{\Delta H}{RT}, \tag{12}$$

$$\Delta G^0 = \Delta H^0 - T\Delta S^0, \tag{13}$$

where K_d, q_e, and c_e are the equilibrium constant, the amount of dye adsorbed on the adsorbent of the solution at equilibrium (mol·L^{-1}), and the equilibrium concentration of dye in the solution (mol·L^{-1}), respectively. ΔG^0 is the free energy change (kJ/mol), ΔH^0 (kJ/mol) and ΔS^0 (J/mol/K) are standard enthalpy and standard entropy. R is the ideal gas constant (kJ/mol/K), and T is the solution temperature (K) [24].

2.3.2. Orthogonal Experiment. As a kind of material with a controllable structure, the modified ATP-RGO composite aerogel has many variables in the preparation process, and each variable restricts the other. The change of a variable will directly affect the performance of the composite aerogel. Therefore, it is necessary to comprehensively analyze the influence of various factors on its performance. Therefore, the orthogonal test method can be used to analyze. The orthogonal experiment method is a design method to study multifactor and multilevel, which can improve the efficiency of the experiment and give the optimization analysis scheme. It is an efficient, rapid, and experimental design method [25]. In this experiment, the solid-liquid ratio of silicon source to alkali solution (A), aging temperature (B), and drying temperature (C) was used as variables to study the influence on the performance of modified ATP-RGO composite aerogel. The orthogonal table L9 (34) of three factors and three levels was selected for nine experiments. The gel time and mechanical strength were tested in the sample preparation process. The results of the orthogonal experiment and analysis are shown in Table 1.

It can be seen from the orthogonal experiment results that the gel of sample 3 ($A_1B_3C_3$) was the fastest. According to the analysis, the primary and secondary order of the factors affecting the gel time was B (aging temperature) > C (drying temperature) > A (solid-liquid ratio), and the primary and secondary order of the factors affecting the mechanical strength was B (aging temperature) > C (drying temperature) > A (solid-liquid ratio). It can be seen that regardless of gel time or mechanical strength, the aging temperature was the most important factor. After measurement, sample 6 ($A_2B_3C_1$) has the highest mechanical strength, which can withstand 100 g weight. It is the best sample in the orthogonal experimental group.

In summary, in the preparation of ATP-RGO CA, the aging temperature has the greatest influence on gelation time and mechanical strength. Analysis of experimental data, comprehensive factors, selected solid-liquid ratio 1 : 15, aging temperature 55°C, drying temperature 40°C, the best preparation process of modified ATP-RGO composite aerogel.

2.3.3. Desorption Experiment. To evaluate the reusability of the composite aerogel, adsorption and desorption tests were conducted using three eluents, namely, 0.01 M CH_3COOH, 0.01 M C_5H_6O, and 0.01 M HCl. Desorption (%) is estimated by

$$\text{desorption (\%)} = \frac{C_m}{C_e} \times 100\%, \tag{14}$$

where C_m and C_e (mg/L) refer to the concentration of MO and MG released in the solution and the initially adsorbed MO and MG concentration, respectively.

3. Discussion

3.1. Material Characterization

3.1.1. X-Ray Diffraction Analysis. XRD diffraction patterns of graphene aerogel and modified ATP-RGO composite aerogel are given in Figure 2. It can be found from the graphene aerogel that a broad diffraction peak appears at $2\theta = 25°$, sharp diffraction peaks disappear, the results showed that the oxygen-containing functional groups on reduced graphene oxide surface were removed by ascorbic acid reduction, and the crystal plane spacing was reduced and the hydrophobicity was enhanced [26]. It was found from the diffraction pattern of the composite aerogel that there was a diffraction peak with small intensity $2\theta = 15° \sim 30°$, and there was no graphene oxide diffraction peak reduced by ascorbic acid. According to JCPDS No. 75-0254, indicating that the composite of silicon oxide and graphene was successful, and it also reflected that in the composite aerogel, amorphous silicon oxide inhibits the natural accumulation of graphene sheets, resulting in an increase in the distance between graphene sheets and the disappearance of graphene diffraction peaks, reflecting the protective effect of amorphous silicon oxide particles [27].

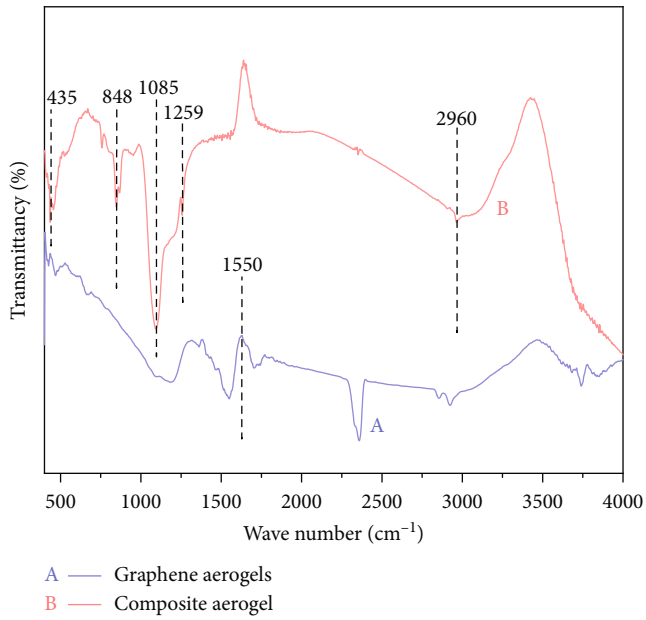

FIGURE 4: Infrared spectra of graphene aerogel and composite aerogel.

3.1.2. Scanning Electron Microscopy. SEM images were used to examine the morphology and structure of graphene aerogels and composite aerogel. Figures 3(a) and 3(b) show the SEM images of graphene aerogels; Figures 3(c) and 3(d) show SEM images of composite aerogel.

It can be seen from Figures 3(a) and 3(b) that the prepared graphene aerogel has a three-dimensional network structure, the graphene sheets overlap with each other, and its structure has a certain regularity. It can be seen from Figures 3(c) and 3(d) that the composite aerogel is also three-dimensional networks. White flake amorphous silicon oxide particles are uniformly distributed on the surface of graphene, indicating that silicon oxide is well loaded on the surface of graphene. These silicon oxide particles coated on the surface can effectively prevent the natural accumulation of graphene oxide sheets, which is another evidence of the protective effect of silicon oxide particles. The existence of a three-dimensional network structure greatly increased the specific surface area of aerogels [28] and provided a large number of adsorption sites, which showed great adsorption capacity.

3.1.3. Infrared Spectroscopic Analysis. From the infrared spectra of graphene aerogel (GA) and composite aerogel (CA) shown in Figure 4, there is no obvious absorption peak, which indicates that the oxygen-containing groups on the graphene aerogel sheet are reduced by ascorbic acid, and the new absorption peak at 1550 cm^{-1} also indicates that the graphene aerogel with the new structure is successfully prepared [29]. The composite aerogel showed characteristic peaks of Si-O-Si at 1085 cm^{-1}, 848 cm^{-1}, and 435 cm^{-1}, indicating that silicon oxide was successfully loaded into the graphene aerogels [30]. Due to the modification of trimethylchlorosilane, the alkyl peak appeared at 2960 cm^{-1}. At 757 cm^{-1} and 2960 cm^{-1}, the antisymmetric stretching

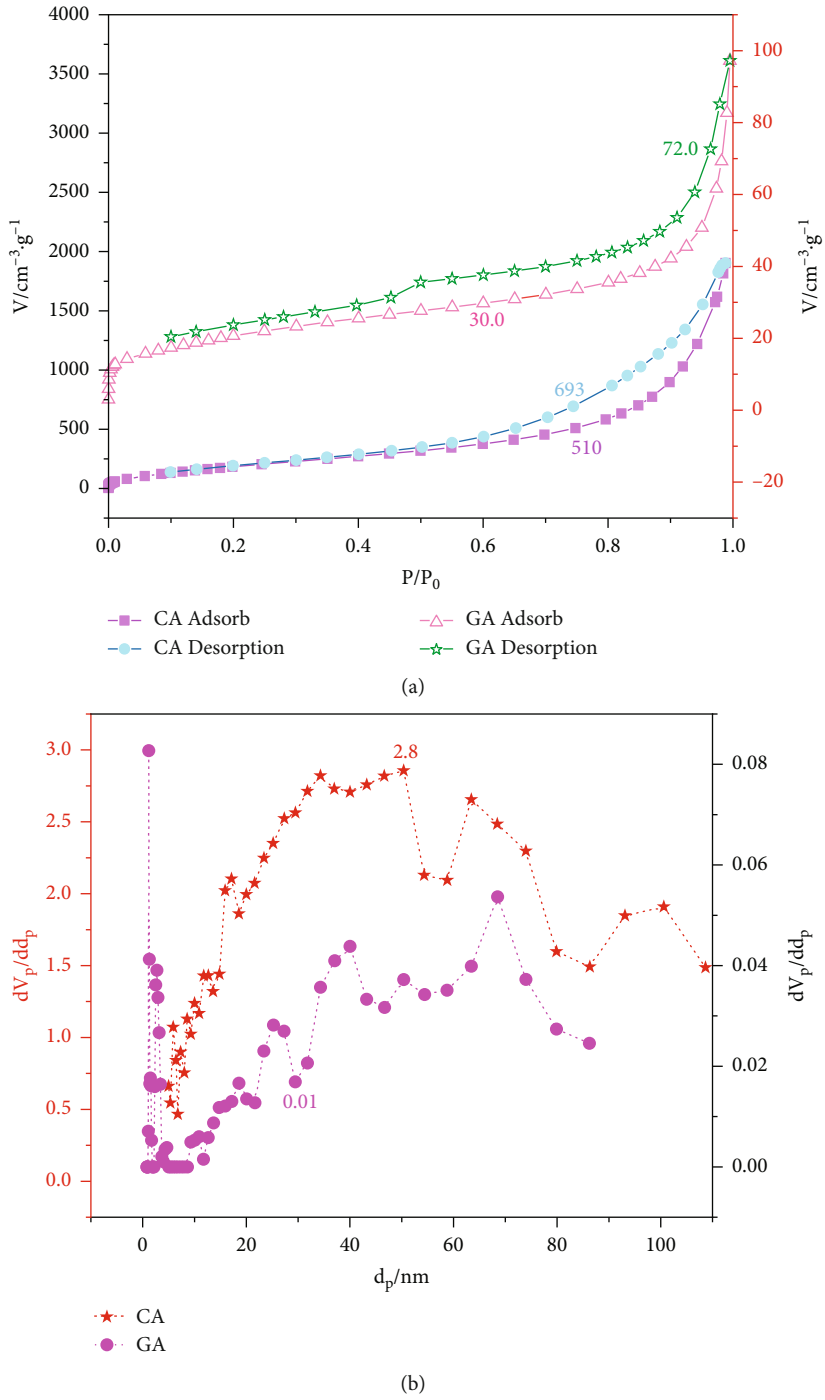

Figure 5: (a) N_2 adsorption-desorption isotherms and (b) pore size distribution of graphene aerogels and composite aerogels.

vibration peak and symmetric stretching vibration peak of C-H in -CH_3 were observed, respectively [31]. The absorption peak near 1259 cm^{-1} was caused by Si-C vibration, which indicated that after the modification of trimethylchlorosilane, -CH_3 was connected to the end branch of the composite aerogel so that the aerogel was hydrophobic [32].

3.1.4. Specific Surface Area and Pore Size Analysis. The N_2 adsorption-desorption isotherms and pore size distribution curves of graphene aerogels and composite aerogel are displayed in Figures 5(a) and 5(b), respectively. From Figure 5(a), it is obvious that all isotherms are type IV, indicating typical mesoporous materials. From Figure 5(b), when $P/P0 > 0.5$, there was an obvious H3 hysteresis loop, indicating that there is a mesoporous structure inside and the pore shape is slender. At this time, the specific surface areas of graphene aerogel and composite aerogel are 171.14 $m^2 \cdot g^{-1}$ and 781.57 $m^2 \cdot g^{-1}$, respectively. –Si–O–C– the

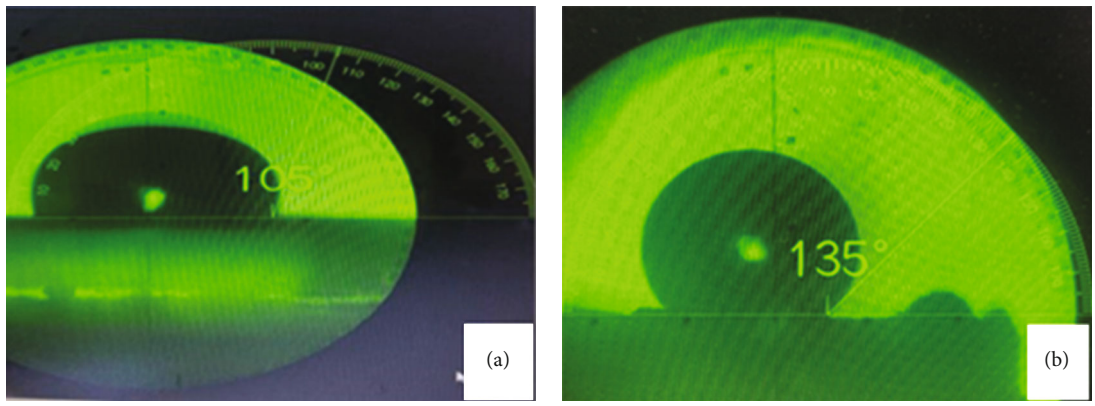

(a) (b)

Figure 6: Contact angle test diagram of (a) graphene aerogel and (b) composite aerogel.

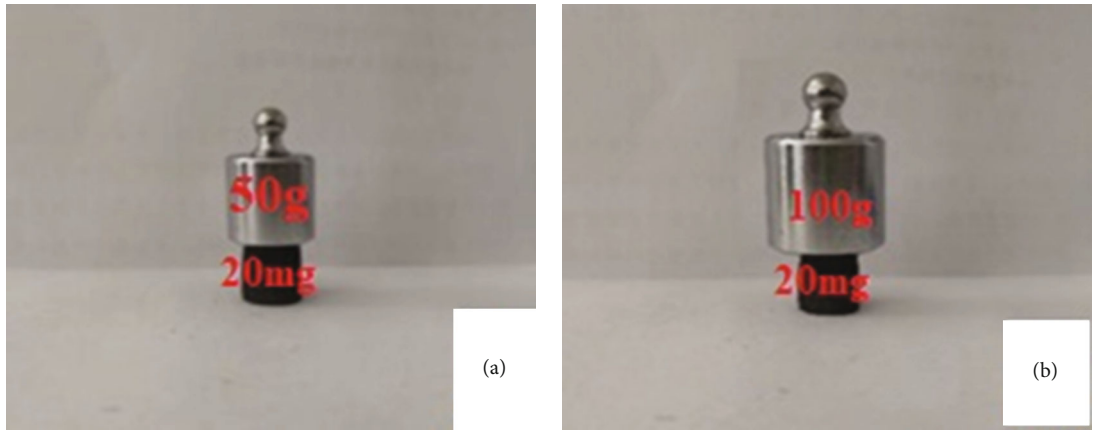

(a) (b)

Figure 7: Mechanical strength test diagram of graphene aerogel and composite aerogel.

bond between amorphous silica compounds and graphene can form via the condensation reaction between –Si–OH and –OH on the basal plane of graphene, where the basal plane of graphene can act as a barrier agent, being favorable to the dispersion of amorphous silica compounds nanoparticles and avoid the formation of large particles, thus resulting in the increase of the specific surface area of aerogels [33]. According to the BET method and BJH equation, the pore volumes of graphene aerogel and composite aerogel are $0.127\,cm^3{\cdot}g^{-1}$ and $2.94\,cm^3{\cdot}g^{-1}$, respectively, and the pore sizes are 2.34 nm and 31.81 nm, respectively. This is mainly due to the successful addition of silica compounds, increasing the spacing of graphene sheets, resulting in increased specific surface area and pore volume [34].

3.1.5. Contact Angle Analysis. The contact angle test diagram of graphene aerogel and composite aerogel is shown in Figures 6(a) and 6(b), respectively. When the contact angle is in the range of 90°~150°, the solid surface is difficult to be soaked in water, which is called the hydrophobic surface and reflects the hydrophobicity of the solid. As shown in the figure, the contact angle between graphene aerogel and pure water is 105°, showing a certain hydrophobicity. The contact angle between the composite aerogel and pure water is 135°, indicating that the sample has good hydrophobicity. Hydrophobicity enables aerogels to maintain nonwettability in water and to preferentially adsorb dyes in water, which is beneficial to the treatment of dye wastewater.

3.1.6. Mechanical Strength Analysis. Aerogels must have a certain mechanical strength, otherwise under the impact of the fluid will appear scattered, structural collapse, and so on. To this end, we tested the mechanical properties of graphene aerogels and composite aerogel, as shown in Figure 7. It indicates that 20 mg of graphene aerogel can support the 2500-fold weight (50 g) of its mass without deformation and damage. Figure 7(b) indicates that 20 mg composite aerogel can successfully support 100 g weight, which is 5000 times its weight. After removing the weight, the aerogel has no deformation and damage, showing excellent mechanical strength. The reason for the increase in the strength of the composite aerogel is that silicon oxide is added as an

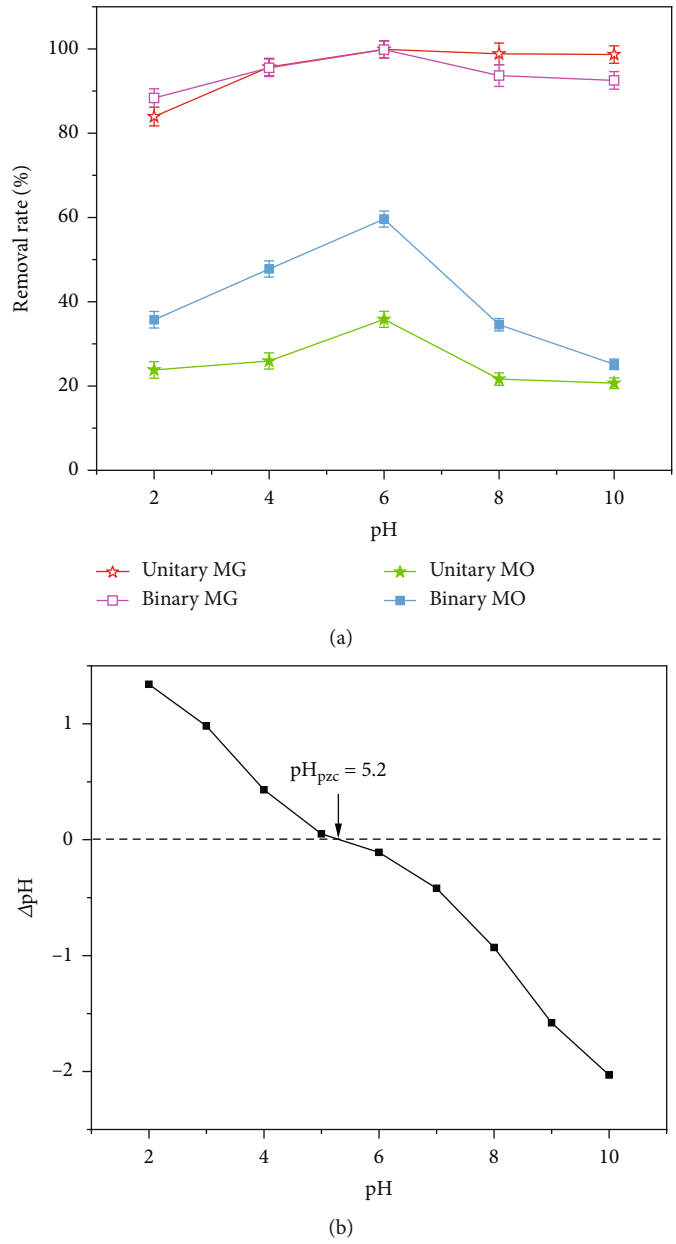

Figure 8: (a) Effect of pH on adsorption of MG and MO; (b) pH_{pzc} of the adsorbent.

agglomeration inhibitor to curb the accumulation of graphene sheets, resulting in a more complete pore wall structure of the composite aerogel, enhancing the stability of its structure and thereby increasing the mechanical strength of the composite aerogel.

3.2. Adsorption Experiments

3.2.1. Effect of pH on Adsorption of Malachite Green and Methyl Orange. The pH is one of the important factors that affect the adsorption process of pollutants in wastewater. The pH influences the solubility of dyes in water, the activity of surface functional groups of the adsorbents, and ion competition for the adsorption centers [35]. To explore the effect of pH on the adsorption properties of composite aerogel, MG and MO monobasic and binary dye systems were adsorbed by composite aerogel under different pH (Figure 8(a)). Meanwhile, to better understand the effect of solution pH on the adsorbent itself, the point of zero charge (pH_{pzc}) of the composite aerogel was also studied. The results are shown in Figure 8(b). The removal rates of MG and MO reached the highest adsorption capacity at pH = 6. Since then, with the increase of pH, the removal rate of MO decreased, but the removal rate of MG remained at the highest point. When pH is lower than 4, the removal rate of MG in the unitary dye system is relatively low, because under acidic conditions, excessive H^+ and cationic dye MG produce competitive adsorption [36]. When pH

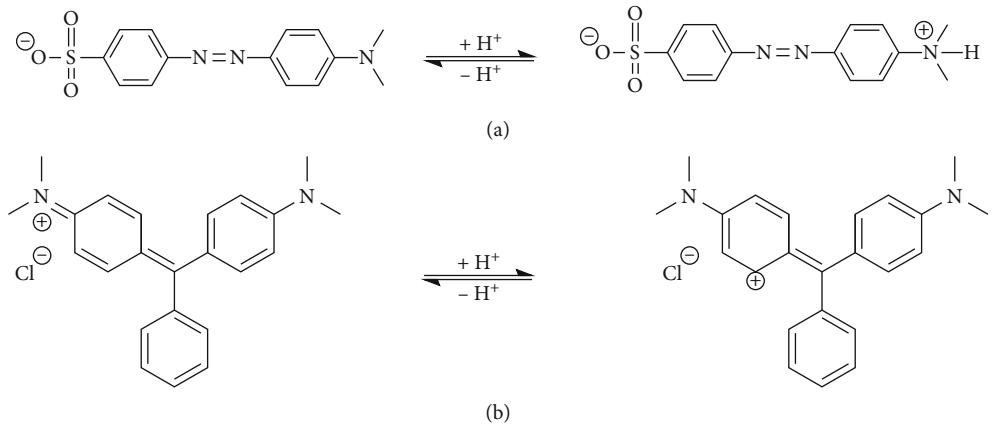

Figure 9: The MO structures in acidic solute (a); the MG structures in acidic solute (b).

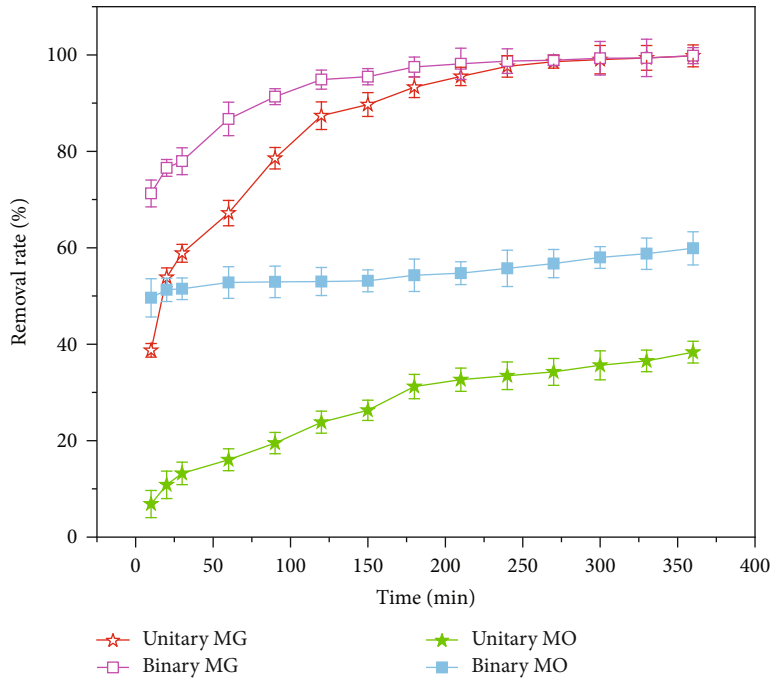

Figure 10: Effect of adsorption time on the adsorption of MG and MO by composite aerogel.

is less than 6, the removal rate of MO increases with the increase of pH. When pH is greater than 6, the removal rate decreases with the increase of pH. This is due to the quinoid structure of methyl orange in an acidic environment. The sulfonic acid end of the molecule is negatively charged, and it can form a chemical bond with MOH_2^+ (Figure 9(a)), which promotes the adsorption of methyl orange to a certain extent. In an alkaline environment, methyl orange is negatively charged and repels MO^-, which hinders the adsorption of methyl orange [37]. And as shown in Figure 8(b), the pH_{pzc} of the composite aerogel is 5.2, which means that the surface of the composite aerogel is negatively charged when the solution pH is greater than 5.2 and positively charged when the solution pH is lower than 5.2. MO is a typical anionic dye with a negative charge. This means that when pH is greater than 5.2, there is electrostatic repulsion between the negatively charged surface and negatively charged MO, which is not conducive to the adsorption of MO [38]. Therefore, with the increase of pH, the removal rate of MO decreased. In contrast, MG is a typical cationic dye, and the increase of pH is beneficial to the adsorption of MG (Figure 9(b)).

Considering the practical application, the pH value was determined to be 6. Different from the monobasic system, the removal rate of MO by composite aerogel in the binary dye system has been greatly improved, indicating that the coexistence of the two dyes has a great role in promoting the adsorption of the two, and the two are synergistic adsorption.

3.2.2. Effect of Adsorption Time on Adsorption of Malachite Green and Methyl Orange. The composite aerogels were

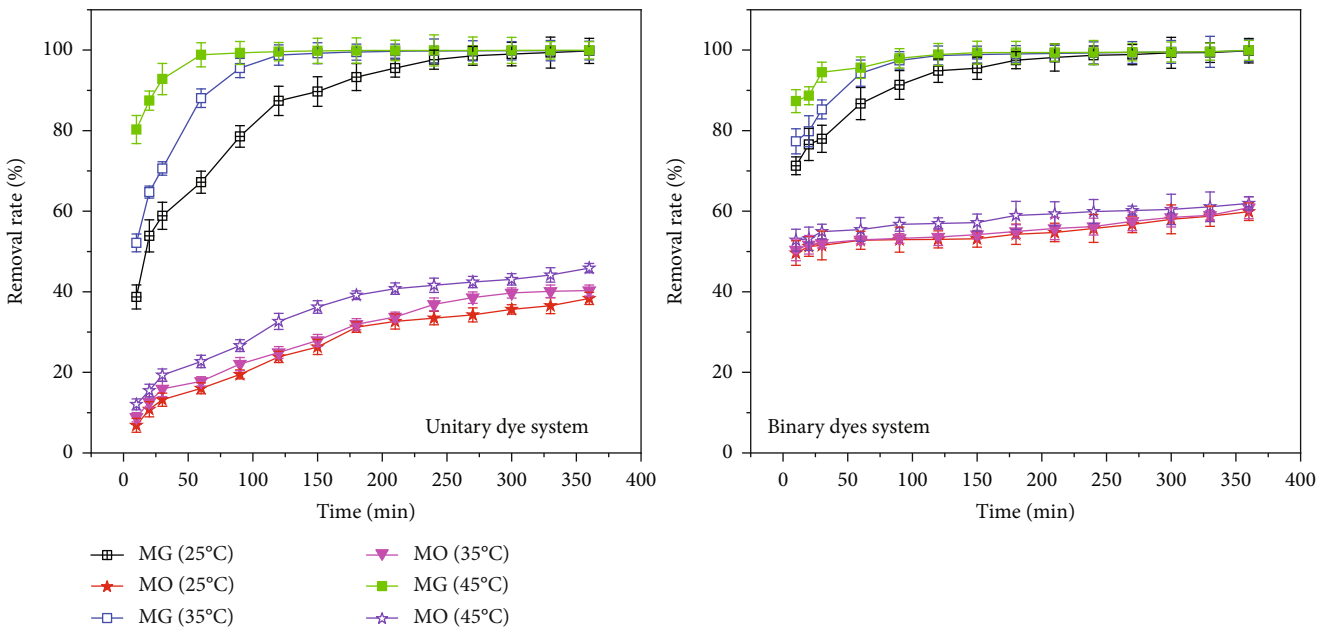

Figure 11: Effect of temperature on the adsorption of MG and MO by composite aerogel.

used to adsorb MG and MO monobasic and binary dye systems, and the results are shown in Figure 10. The removal rate of MG by composite aerogel in either monobasic or binary dye systems was high, indicating that the silica compounds were successfully composited into graphene aerogels, which increased the specific surface area of composite aerogel and improved their adsorption capacity. It can be seen that in the binary system, MG and MO reach the adsorption equilibrium after 180 and 60 minutes, respectively, while in the unitary system, MG and MO reach the adsorption equilibrium after 250 minutes. At the same time, the removal rates of MG and MO in the binary dye system were higher than those in the monadic system, which was due to the formation of dimers between MG and MO in the binary system to improve their aromaticity, thereby enhancing the π-π interaction between themselves and the adsorbent and improving the adsorption performance of MG. When MG is adsorbed on the surface of the adsorbent, the electrostatic repulsion between the adsorbent surface and the MO molecule will be weakened. At the same time, the adsorbed MG forms hydrogen bonds or π-π interactions with the MO in the solution, thereby enhancing the interaction between the two and thereby improving the removal rate of MO in the binary dye system [39].

3.2.3. Effect of Adsorption Temperature on Adsorption of Malachite Green and Methyl Orange. At different temperatures, MG and MO monobasic and binary dye systems were adsorbed to explore the effect of temperature on the adsorption properties of composite aerogel. The results are shown in Figure 11. The removal rate of MG and MO increased with the increase in temperature, indicating that the adsorption of dyes by composite aerogel was an endothermic reaction. It is obvious that in the binary system, the removal rate of MO by composite aerogel fluctuates little with time, and the removal rate is much higher than that of the monobasic dye system, which once again shows the synergistic adsorption of the two dyes. In addition, it can be observed that the removal rate of MG by composite aerogel in the binary dye system is higher than that in the unitary system, which also reflects that MG and MO form dimers to improve their aromaticity in the binary system, thereby enhancing the π-π interaction between themselves and the adsorbent and improving the adsorption performance of MG [39].

3.2.4. Adsorption Kinetics of Malachite Green and Methyl Orange on Modified ATP-RGO Composite Aerogel. To explore the adsorption mechanism of MG and MO on composite aerogel, pseudo-first-order kinetic model, pseudo-second-order kinetic model, and intraparticle diffusion model were used to fit and analyze the experimental results of MG and MO adsorption on monobasic and binary dye systems. The obtained adsorption kinetics data are shown in Figure 12 and Table 2.

Table 2 shows the fitting of different kinetic equations to the test results. According to the data in the table, the correlation coefficient R^2 of the fitting quasi-second-order kinetic equation is greater than that of the fitting quasi-first-order kinetic equation and is greater than 0.999, indicating that the adsorption process of dyes on composite aerogel is more in line with the quasi-second-order kinetic equation. It indicates that adsorption is a chemical process, not a physical diffusion process. In addition, it can be seen from the quasi-second-order kinetic parameters that in the binary dye system, the parameter q_e of MG is significantly smaller than that of the mono-dye system, while the parameter q_e of MO is significantly higher than that of the mono-dye system. This is because, in the binary dye system, the presence of MG promotes the adsorption of MO by the composite aerogel. In the table, the linear correlation coefficient obtained by

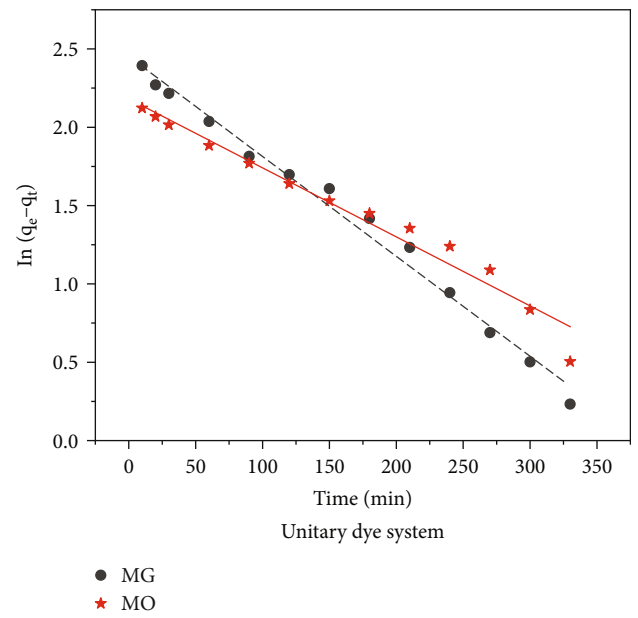

(a)

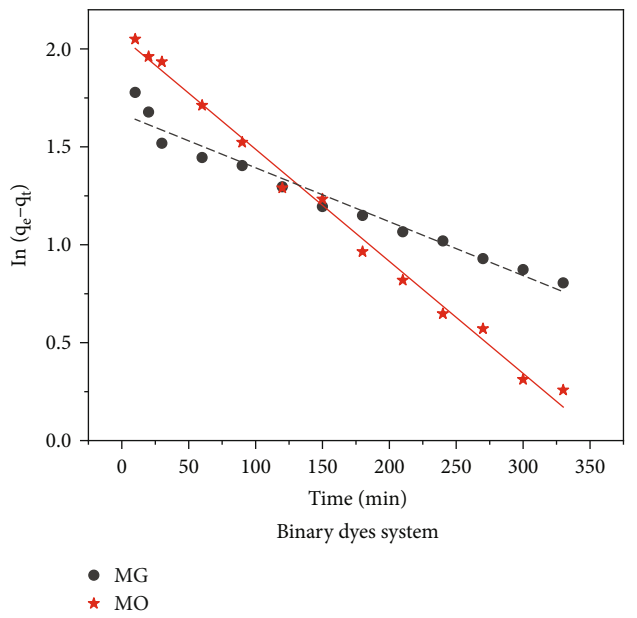

(b)

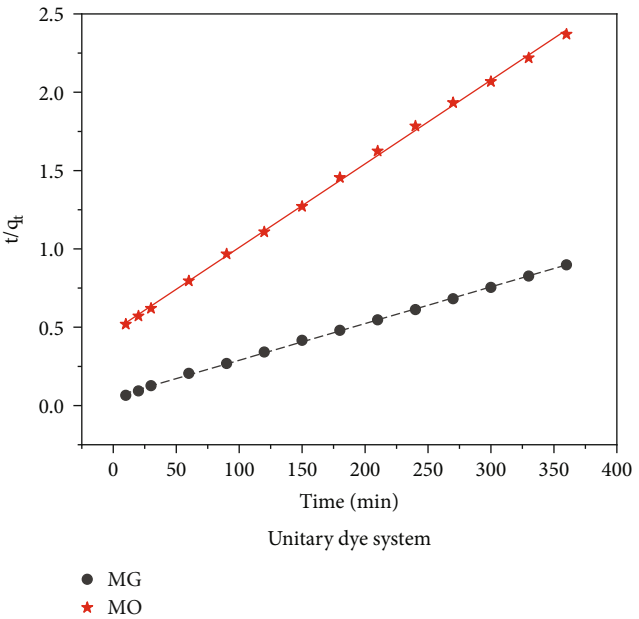

(c)

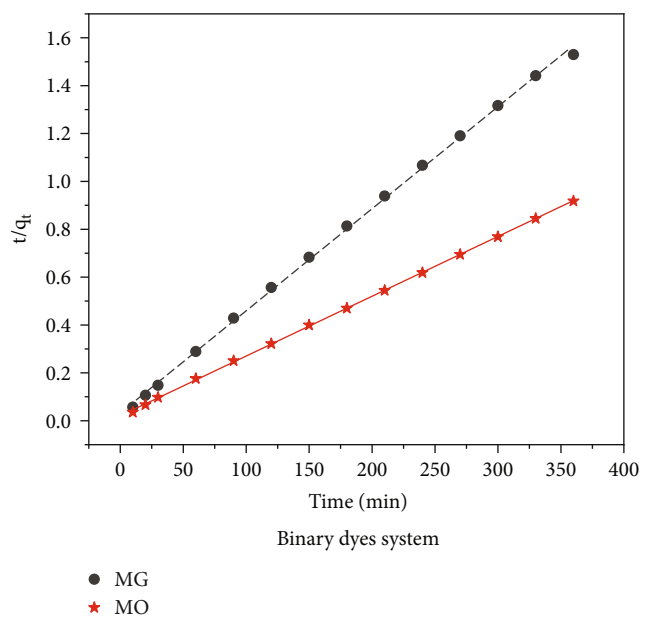

(d)

Figure 12: Continued.

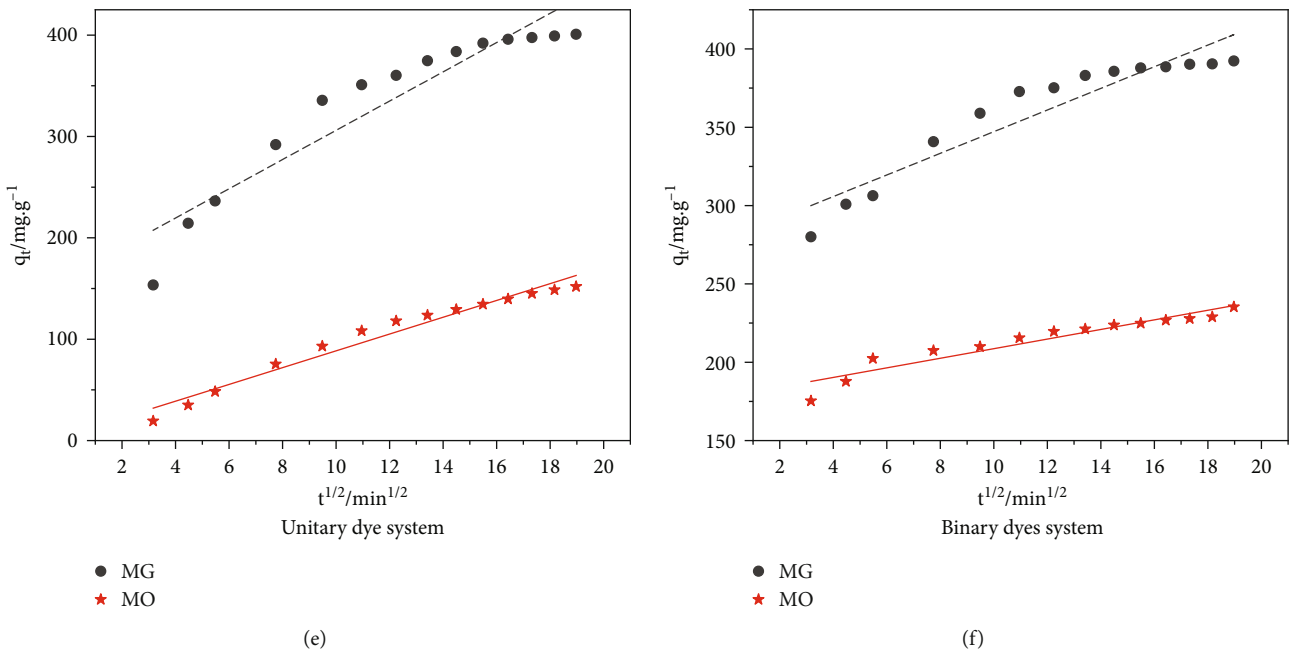

Figure 12: (a, b) Pseudo-first-order kinetic fitting curve, (c, d) pseudo-second-order kinetic fitting curve, and (e, f) intraparticle diffusion equation fitting curve of MG and MO adsorption on composite aerogel.

Table 2: Adsorption kinetic parameters of malachite green and methyl orange on composite aerogel.

		Pseudo-first-order kinetic equation			Pseudo-second-order kinetic equation			Intraparticle diffusion equation	
		K_1 (min^{-1})	q_e (mg·g^{-1})	R^2	$K_2 \times 10^{-3}$ (g·mg^{-1}·min^{-1})	q_e (mg·g^{-1})	R^2	K_p (mg·(g·s)$^{-1}$)	R^2
MG	Unitary	0.006	11.6	0.989	0.096	434.78	0.9994	14.4	0.894
	Binary	0.006	7.85	0.993	0.0003	400.00	0.9998	6.91	0.889
MO	Unitary	0.004	8.86	0.969	0.0592	188.68	0.9992	8.28	0.966
	Binary	0.003	5.30	0.964	0.0006	232.56	0.9991	3.07	0.907

particle diffusion fitting is very low, indicating that the particle diffusion equation cannot fully describe the whole adsorption process and should be controlled by the combination of particle diffusion and membrane diffusion [40, 41].

3.2.5. Adsorption Isotherms of Malachite Green and Methyl Orange on Modified ATP-RGO Composite Aerogel. To explore the interaction between composite aerogel and two dyes, unitary and binary dye systems with different initial concentrations were adsorbed at 25°C and an analysis of adsorption isotherm. The adsorption isotherm data fitted by Langmuir, Freundlich, and Temkin isotherm models are tabulated in Figure 13 and Table 3.

As shown in Table 3, based on the Langmuir isotherm model data, under the optimum experimental conditions (temperature = 25°C, initial concentration = 200 mg/L, adsorption time = 360 min), the maximum adsorption capacity of the binary dye system is better than that of unitary dye system, the maximum adsorption capacity of MG and MO in the binary dye system was 842.0 mg/g and 540.5 mg/g, respectively. In Table 4, we compared the maximum adsorption capacities of MG and MO on the adsorbents proposed in this study with those in other studies. The results show that the adsorbent proposed in this study has higher adsorption capacity for MG and MO.

It can be seen from Table 3 that the R^2 coefficient fitted by the Langmuir isothermal equation was higher than that fitted by the Freundlich isothermal and Temkin isothermal, which was greater than 0.99, indicating that the Langmuir isothermal adsorption equation was more in line with the adsorption process of composite aerogel for dyes, indicating that the adsorption process belonged to monolayer adsorption, and the surface structure of the adsorbent was uniform [46]. Meanwhile, the dimensionless separation factor R_L of the Langmuir model can effectively reflect the adsorption process: when $R_L > 1$, it indicates that the adsorption is not favorable; when $R_L = 1$, the adsorption is linear; when $0 < R_L < 1$, the adsorption is favorable, and if $R_L = 0$, it means that adsorption is irreversible. As shown in Table 3, the R_L values of the two dyes are all between 0 and 1 in both unitary and binary systems. It shows that the adsorption of two dyes on composite aerogel is favorable and reversible. In addition, in the Freundlich model values, $n < 1$ indicated that adsorbate was unfavorably adsorbed on an adsorbent, while $n >$

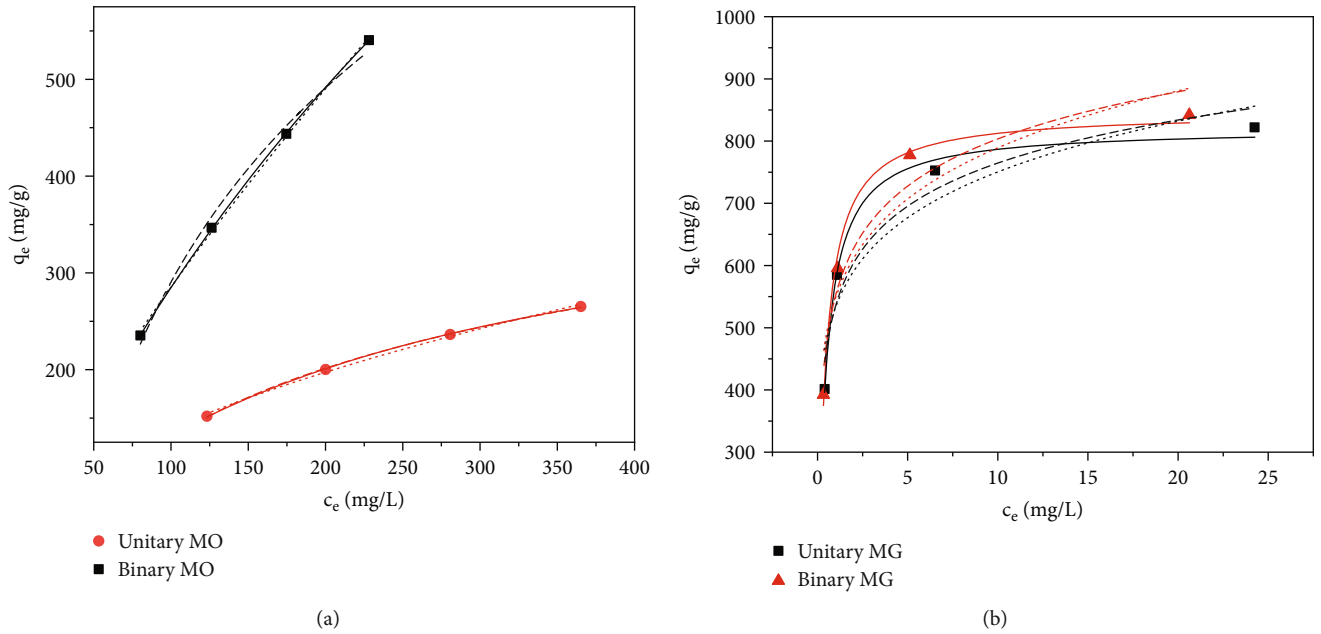

Figure 13: Isotherm fittings of (a) MO adsorption and (b) MG adsorption on the composite aerogels (Langmuir isotherm: solid line, Freundlich isotherm: point line, Temkin isotherm: scratch line).

Table 3: Adsorption isotherm parameters of MG and MO on composite aerogel.

		Langmuir isothermal				Freundlich isothermal			Temkin isothermal		
		Q_m	k	R_L	R^2	n	K_F	R^2	k_T	f	R^2
MG	Unitary	822.1	0.053	0.87	0.99	1.48	14.9	0.91	98.93	0.04	0.95
	Binary	842.0	0.024	0.17	0.99	1.46	1.68	0.90	105.5	0.03	0.92
MO	Unitary	365.3	0.004	0.55	0.99	1.69	13.1	0.99	104.3	0.21	0.99
	Binary	540.5	0.002	0.73	0.99	1.27	7.80	0.99	109.6	0.16	0.99

Table 4: Comparison of maximum adsorption capacities of different adsorbents for MG and MO.

Dye	Adsorbent	Maximum adsorption capacity ($mg \cdot g^{-1}$)	Reference
MG	Cd $(OH)_2$-NW-AC	80.64	[42]
	NiO flowerlike nanoarchitectures	142.1	[43]
	$NiFe_2O_4$ NPs	210.0	[14]
	ATP-RGO CA	842.0	This study
MO	$CoFe_2O_4$ from binary solutions with CR	117.5	[35]
	Muscovite-supported Fe_3O_4 nanoparticles	149.3	[44]
	Multiwalled carbon nanotubes (MWCNTs) coated	81.00	[45]
	ATP-RGO CA	540.5	This study

1 indicated that adsorbate was favorably adsorbed on an adsorbent [47]. In this study, the n value was higher than 1, which indicated that adsorption intensity was good throughout the experimental concentration range. Finally, the fitted R^2 values of the Temkin model in unitary and binary systems of MG and MO are relatively high, suggesting that there is a strong electrostatic interaction between MG, MO, and composite aerogel which contributes to adsorptive removal of both dyes[48–52].

3.2.6. Adsorption Thermodynamics Analysis of Malachite Green and Methyl Orange on Modified ATP-RGO Composite Aerogel. The thermodynamic parameters of MG and MO adsorption by composite aerogel at 298.15 K, 308.15 K, and 318.15 K were obtained through the thermodynamic analysis of the adsorption process of MG and MO in the monobasic and binary dye systems. The results are shown in Table 5. All $\triangle G^0$ was less than 0 and greater than −20 kJ/mol, indicating that the adsorption reaction was

Table 5: Adsorption thermodynamic parameters of MG and MO on composite aerogel.

	T (K)		$\triangle G^0$ (kJ·mol^{-1})		$\triangle H^0$ (KJ·mol^{-1})		ΔS^0 (J·mol^{-1}·K^{-1})	
	Unitary	Binary	Unitary	Binary	Unitary	Binary	Unitary	Binary
MG	298.15 K	298.15 K	-7.30	-7.56	23.4	17.2	102.81	83.1
	308.15 K	308.15 K	-8.33	-8.39				
	318.15 K	318.15 K	-9.36	-9.22				
MO	298.15 K	298.15 K	-0.20	-1.16	5.23	1.54	18.21	9.05
	308.15 K	308.15 K	-0.38	-1.25				
	318.15 K	318.15 K	-0.56	-1.34				

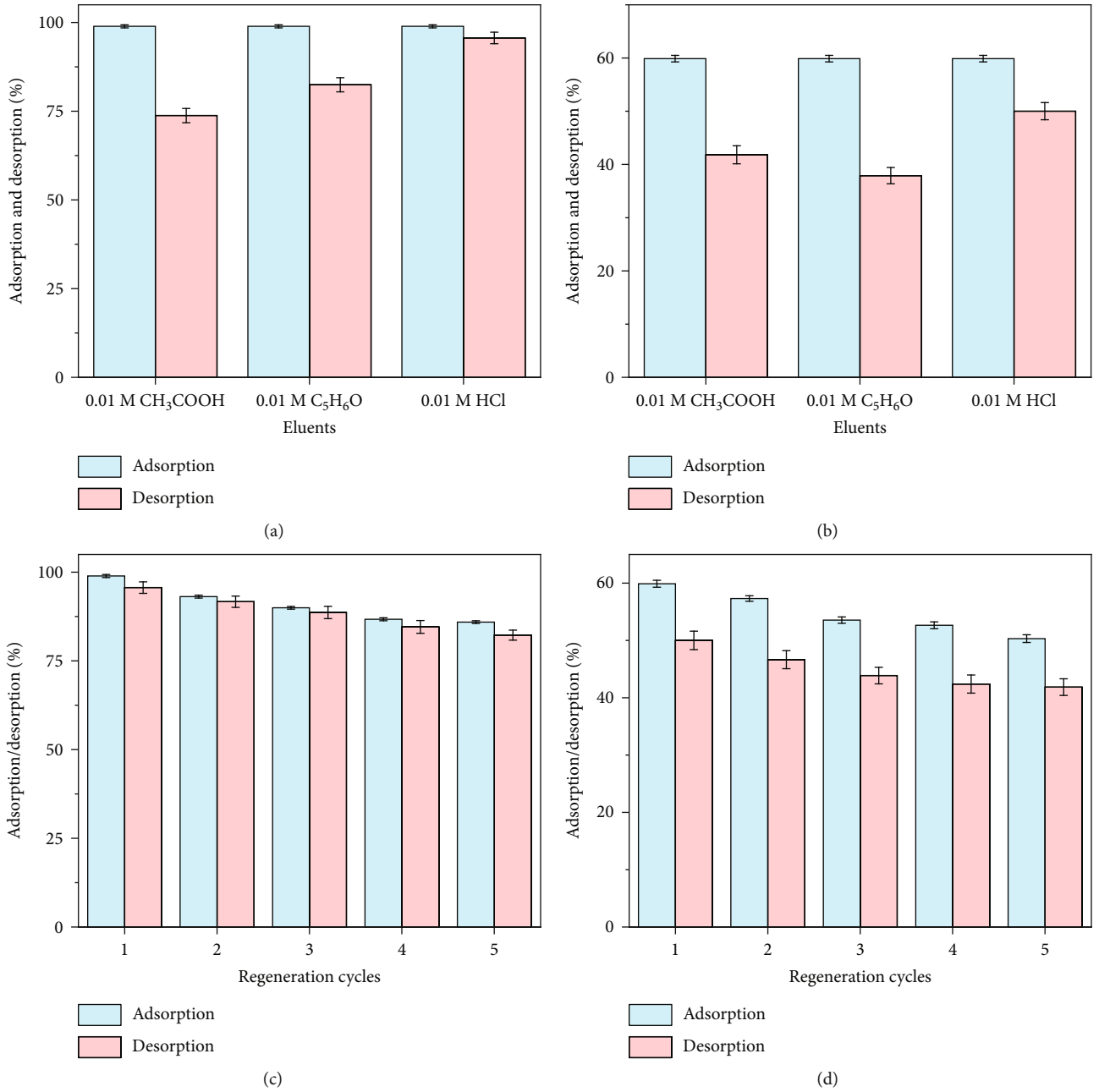

Figure 14: (a) Comparison of eluents for desorption of MG from composite aerogel surface, (b) comparison of eluents for desorption of MO from composite aerogel surface, and reusability of composite aerogel for (c) MG and (d) MO.

spontaneous [53]. The absolute value of ΔG^0 increases with the increase of ambient temperature, indicating that the degree of spontaneity increases with the increase of temperature [54]. The positive value of ΔS^0 indicates that the adsorption process is an entropy increase process, and the randomness at the solid-solution interface occurs in the internal structure of the adsorption of MG and MO dyes onto composite aerogel [55]. Table 5 also shows that $\triangle H^0$ of composite aerogel is greater than 0 in the either monobasic or binary system, indicating that the adsorption process is an endothermic reaction and $\triangle H^0$ of the binary dye system is less than that of the unitary dye system, which further confirms the existence of MG, promotes the adsorption of MO by composite aerogel, and reduces the difficulty of adsorption.

3.2.7. Desorption Study. Nowadays, the reproduction of adsorbents is one of the most challenging and important factors for industrial applications. At the same time, the reusability is also one of the criteria for evaluating the performance of an adsorbent. In this study, 0.01 M CH_3COOH, 0.01 M C_5H_6O, and 0.01 M HCl were designated as desorbing agents to test the reusability of composite aerogel in multiple dye adsorption-desorption cycles. Five adsorption-desorption cycles in ethanol, acetone, and HCl were applied to check the reusability of both adsorbents. The results of these experiments are presented in Figure 14.

As shown in Figure 14, the desorption process of MG and MO loaded on composite aerogel was performed by 0.01 M ethanol, 0.01 M acetone, and 0.01 M HCl as three eluents by an ultrasonic assistant. Readsorption process was carried out at the same optimum condition of experiments (pH = 6, adsorbent dosage = 0.02 g, initial concentration = 200 mg/L, and mixing time = 360 min). The composite aerogel was washed several times with eluent by ultrasonic aid until the most of dye molecules were extracted from the surface of the composite [35, 48]. At last, the recovered composite aerogel before being dried in a vacuum oven at 70°C was rinsed one more time with distilled water. It was found that 0.01 M HCl had the best desorption effect on MG and MO compared with the other two eluents, so HCl was selected as the eluent for subsequent cycle experiments.

After five cycles, the adsorption amount of MG on the composite aerogel decreased by 13.4%, and the final adsorption amount was 82.27%. The adsorption amount of MO decreased by 8.15%, and the final adsorption amount was 41.86% (Figures 12(c) and 12(d)). The results indicated that composite aerogel was a regenerable and reusable adsorbent.

4. Conclusions

The modified attapulgite-reduced graphene oxide composite aerogel (ATP-RGO CA) was synthesized by the sol-gel method to be used as effective adsorbents for the removal of malachite green (MG) and methyl orange (MO) dyes from unitary and binary aqueous solutions. The as-obtained composite materials prepared were characterized by X-ray diffraction, FTIR spectroscopy, SEM, and specific surface area and porosity analysis. The results confirmed the successful synthesis of composite materials. Moreover, the physical properties of the prepared composite aerogel were improved compared with those of the initial graphene aerogels. Kinetic, equilibrium, and thermodynamic studies were conducted for the adsorption of MG and MO from aqueous solutions onto ATP-RGO CA in unitary and binary systems. The results of adsorption showed that ATP-RGO CA can be effectively used as an adsorbent for the removal of dyes. The kinetic studies of dyes on ATP-RGO CA were performed based on pseudo-first-order, pseudo-second-order, and intraparticle diffusion rate mechanisms. The data indicated that the adsorption kinetics of dyes on ATP-RGO CA followed the pseudo-second-order model. The equilibrium data were analyzed using the Langmuir, Freundlich, and Temkin isotherms, and the characteristic parameters for each isotherm were determined. The results showed that the Langmuir isotherm best describes the adsorption on ATP-RGO CA and indicates that MG and MO adsorption occurs on the homogeneous surface of ATP-RGO CA as a monolayer. Thermodynamic studies show that the adsorption process of MG and MO onto ATP-RGO CA was endothermic and spontaneous. The reusability test of ATP-RGO CA exhibited that the adsorption capacity of ATP-RGO CA decreased slightly after five cycles, but the adsorption capacity was still good. The results of the study indicate that ATP-RGO CA is relevant as adsorbent to clean dye-containing wastewater.

Data Availability

All relevant data in this article are available to the corresponding author.

Conflicts of Interest

The authors state that there is no conflict of interest in the publication of this paper.

Acknowledgments

This work was supported by the National Natural Science Foundation of China (No. 21573171), the Shaanxi Province Key Research and Development Plan of China (2021SF-438), the Natural Science Foundation of Shaanxi Province of China (No. 17JK0327), the Ph.D. Research Initiation Fund of Xi'an Polytechnic University (BS201932), and the Research and Innovation Training Project for Graduate in General Universities of China (201910709028).

References

[1] J. Liu, Q. X. Zhu, X. W. Tan, Y. Yan, and H. P. Zhang, "Adsorption of methyl orange on modified activated carbon," *The Chinese Journal of Process Engineering*, vol. 16, pp. 222–227, 2016.

[2] L. G. Silva, R. Ruggiero, P. M. Gontijo, R. B. Pinto, and B. Royer, "Adsorption of Brilliant Red 2BE dye from water solutions by a chemically modified sugarcane bagasse lignin," *Chemical Engineering Journal*, vol. 168, no. 2, pp. 620–628, 2011.

[3] S. Liu, Y. Ding, P. Li et al., "Adsorption of the anionic dye Congo red from aqueous solution onto natural zeolites modified with N,N-dimethyl dehydroabietylamine oxide," *Chemical Engineering Journal*, vol. 248, pp. 135–144, 2014.

[4] K. G. Pavithra, P. S. Kumar, V. Jaikumar, and P. S. Rajan, "Removal of colorants from wastewater: a review on sources and treatment strategies," *Journal of Industrial and Engineering Chemistry*, vol. 75, pp. 1–19, 2019.

[5] H. Chen, Y. F. Liu, X. Q. Xu et al., "How does iron facilitate the aerated biofilter for tertiary simultaneous nutrient and refractory organics removal from real dyeing wastewater," *Water Research*, vol. 148, pp. 344–358, 2019.

[6] P. S. Kumar, S. Ramalingam, C. Senthamarai, M. Niranjanaa, P. Vijayalakshmi, and S. Sivanesan, "Adsorption of dye from aqueous solution by cashew nut shell: studies on equilibrium isotherm, kinetics and thermodynamics of interactions," *Desalination*, vol. 261, no. 1-2, pp. 52–60, 2010.

[7] A. Alinsafi, M. Khemis, M. N. Pons et al., "Electro-coagulation of reactive textile dyes and textile wastewater," *Chemical Engineering and Processing: Process Intensification*, vol. 44, no. 4, pp. 461–470, 2005.

[8] E. Sharifpour, M. Ghaedi, A. Asfaram, M. Farsadrooh, E. A. Dil, and H. Javadian, "Modeling and optimization of ultrasound-assisted high performance adsorption of Basic Fuchsin by starch-capped zinc selenide nanoparticles/AC as a novel composite using response surface methodology," *International Journal of Biological Macromolecules*, vol. 152, pp. 913–921, 2020.

[9] R. K. Sonwani, G. Swain, B. S. Giri, R. S. Singh, and B. N. Rai, "Biodegradation of Congo red dye in a moving bed biofilm reactor: performance evaluation and kinetic modeling," *Bioresource Technology*, vol. 302, article 122811, 2020.

[10] M. Cheng, G. Zeng, D. Huang et al., "Efficient degradation of sulfamethazine in simulated and real wastewater at slightly basic pH values using Co-SAM-SCS/H_2O_2 Fenton-like system," *Water Research*, vol. 138, pp. 7–18, 2018.

[11] B. Hameed and T. Lee, "Degradation of malachite green in aqueous solution by Fenton process," *Journal of Hazardous Materials*, vol. 164, no. 2-3, pp. 468–472, 2009.

[12] L. Ai and J. Jiang, "Removal of methylene blue from aqueous solution with self-assembled cylindrical graphene-carbon nanotube hybrid," *Chemical Engineering Journal*, vol. 192, pp. 156–163, 2012.

[13] X. Li, T. Liu, and D. Wang, "Superlight adsorbent sponges based on graphene oxide crosslinked with poly (vinyl alcohol) for continuous flow adsorption," *ACS Applied Materials & Interfaces*, vol. 10, no. 25, pp. 21672–21680, 2018.

[14] S. Sobhanardakani, R. Zandipak, H. Khoshsafar, and R. Zandipak, "Removal of cationic dyes from aqueous solutions using $NiFe_2O_4$ nanoparticles," *Journal of Water Supply: Research and Technology—AQUA*, vol. 65, pp. 64–74, 2015.

[15] H. J. Wu, H. Y. Hu, Q. L. Chen, J. Wang, and L. Xiang, "Preparation of low-density hydrophobic silica aerogels by controlling strength of alcogels," *CIESC Journal*, vol. 66, pp. 4281–4287, 2015.

[16] Y. Cheng, Q. X. Zhou, and Q. Y. Ma, "Progress in treating methods of wastewater containing dyes," *Techniques And Equipment for Environmental Pollution Control*, vol. 4, pp. 56–60, 2003.

[17] N. Q. Ren, X. J. Zhou, and W. Q. Guo, "A review on treatment methods of dye wastewater," *CIESC Journal*, vol. 64, pp. 84–94, 2013.

[18] S. Y. Li, F. Xiong, L. Wang, Y. Wang, and S. B. Xie, "Adsorption properties of graphene oxide/SiO2 composites for Cd(II)," *Acta Materiae Compositae Sinica*, vol. 34, pp. 1205–1211, 2017.

[19] C. Yang, Z. Du, M. Z. Li, and Y. Zhang, "Preparation and influencing factors of the 3-D graphene," *Micronanoelectronic Technology*, vol. 52, pp. 521–525, 2015.

[20] Y. Zhang, *Adsorption properties of graphene oxide composite aerogels for Cd and MB*, Northwest A&F University, China, 2019.

[21] H. J. Li, X. D. Zhou, H. B. Gao, and L. J. Chen, "Influence of different modification methods on pore structure and $Cr6^+$ adsorption of ATP," *Chemical Engineering*, vol. 45, pp. 29–33, 2017.

[22] X. Z. Zhou, *Synthesis of zeolites from attapulgite clay and its applications*, Zhejiang University, China, 2013.

[23] I. Bameri, J. Saffari, S. Baniyaghoob, and M. S. Ekrami-Kakhki, "Synthesis of magnetic nano-$NiFe_2O_4$ with the assistance of ultrasound and its application for photocatalytic degradation of Titan Yellow: kinetic and isotherm studies," *Colloid and Interface Science Communications*, vol. 48, article 100610, 2022.

[24] N. M. Mahmoodi, "Nickel ferrite nanoparticle: synthesis, modification by surfactant and dye removal ability," *Water, Air, and Soil Pollution*, vol. 224, no. 2, p. 1419, 2013.

[25] K. Chen, *Design and analysis of experiment*, Tsinghua University publishing house, China, 2005.

[26] M. Ren, Z. Q. Qu, X. Tan, and C. L. Jiao, "Preparation of PDMS/Fe_3O_4/graphene aerogel composite and its application in oil-water separation," *Research of Environmental Sciences*, vol. 34, pp. 2173–2181, 2021.

[27] J. C. Xu, B. Zhang, Y. K. Lu et al., "Adsorption desulfurization performance of PdO/SiO_2@graphene oxide hybrid aerogel: influence of graphene oxide," *Journal of Hazardous Materials*, vol. 421, article 126680, 2022.

[28] Y. Wu, H. Luo, H. Wang, C. Wang, J. Zhang, and Z. Zhang, "Adsorption of hexavalent chromium from aqueous solutions by graphene modified with cetyltrimethylammonium bromide," *Journal of Colloid and Interface Science*, vol. 394, pp. 183–191, 2013.

[29] T. T. P. N. Trinh, D. M. Nguyet, T. H. Quan et al., "Preparing three-dimensional graphene aerogels by chemical reducing method: investigation of synthesis condition and optimization of adsorption capacity of organic dye," *Surfaces and Interfaces*, vol. 23, article 101023, 2021.

[30] S. Caprarescu, C. Modrogan, V. Purcar, and A. M. Dancila, "Study of polyvinyl alcohol-SiO_2 nanoparticles polymeric membrane in wastewater treatment containing zinc ions," *Polymers*, vol. 13, no. 11, article 1875, 2021.

[31] J. A. Labinger and J. E. Bercaw, "Understanding and exploiting C-H bond activation," *ChemInform*, vol. 417, no. 6888, pp. 507–514, 2002.

[32] L. Pastewka, A. Klemenz, P. Gumbsch, and M. Moseler, "Screened empirical bond-order potentials for Si-C," *Physical Review B Condensed Matter*, vol. 87, no. 20, article 205410, 2013.

[33] J. Kim, L. J. Cote, F. Kim, W. Yuan, K. R. Shull, and J. Huang, "Graphene oxide sheets at interfaces," *Journal of the American Chemical Society*, vol. 132, no. 23, pp. 8180–8186, 2010.

[34] L. Liu, R. Bao, J. H. Yi, M. Xie, S. D. Guo, and P. Yang, "Preparation and properties of CNTs-graphene aerogel," *Acta Materiae Compositae Sinica*, vol. 34, pp. 2296–2303, 2017.

[35] C. M. Simonescu, A. Tătărus, D. C. Culită, N. Stănică, and I. A. Ionescu, "Comparative study of $CoFe_2O_4$ nanoparticles and $CoFe_2O_4$-chitosan composite for Congo red and methyl orange removal by adsorption," *Nanomaterials*, vol. 11, no. 3, article 711, 2021.

[36] C. R. Girish, "Multicomponent adsorption and the interaction between the adsorbent and the adsorbate: a review," *Interaction*, vol. 14, article 15, 2018.

[37] Q. K. Hu, "Removal of methyl orange from water with fly ash," *Shanghai Chemical Industry*, vol. 8, pp. 10–12, 2004.

[38] W. A. Khanday, M. J. Ahmed, P. U. Okoye, E. H. Hummadi, and B. H. Hameed, "Single-step pyrolysis of phosphoric acid-activated chitin for efficient adsorption of cephalexin antibiotic," *Bioresource Technology*, vol. 280, pp. 255–259, 2019.

[39] J. Ma, Y. Ma, and F. Yu, "A novel one-pot route for large-scale synthesis of novel magnetic CNTs/Fe@C hybrids and their applications for binary dye removal," *ACS Sustainable Chemistry & Engineering*, vol. 6, no. 7, pp. 8178–8191, 2018.

[40] D. Y. Song, H. Q. Guo, and L. S. Yan, "Adsorptive property of crystal violet on camellia oleifera shell in aqueous solution," *Chinese Journal of Environmental Engineering*, vol. 8, pp. 5129–5134, 2014.

[41] Z. Q. Huang, Y. X. Ding, and T. Q. Yang, "Preparation of magnetic microsphere containing quaternary ammonium salt of chitosan and methyl orange adsorption," *New Chemical Materials*, vol. 46, pp. 209–212, 2018.

[42] M. Ghaedi, G. Negintaji, H. Karimi, and F. Marahel, "Solid phase extraction and removal of brilliant green dye on zinc oxide nanoparticles loaded on activated carbon: new kinetic model and thermodynamic evaluation," *Journal of Industrial and Engineering Chemistry*, vol. 20, no. 4, pp. 1444–1452, 2014.

[43] A. Wei, B. Liu, H. Zhao et al., "Synthesis and formation mechanism of flowerlike architectures assembled from ultrathin NiO nanoflakes and their adsorption to malachite green and acid red in water," *Chemical Engineering Journal*, vol. 239, pp. 141–148, 2014.

[44] M. A. Barakat, R. Kumar, E. C. Lima, and M. K. Seliem, "Facile synthesis of muscovite supported Fe_3O_4 nanoparticles as an adsorbent and heterogeneous catalyst for effective removal of methyl orange: characterisation, modelling, and mechanism," *Journal of the Taiwan Institute of Chemical Engineers*, vol. 119, pp. 146–157, 2021.

[45] Y. Zhang and Z. Nan, "Preparation of magnetic $ZnLa_{0.02}Fe_{1.98}O_4$/MWCNTs composites and investigation on its adsorption of methyl orange from aqueous solution," *Materials Research Bulletin*, vol. 66, pp. 176–185, 2015.

[46] Y. X. Ma, P. S. Jin, W. J. Shao, Y. L. Kou, and P. Q. La, "Adsorption behavior of Hg (II) on the hydroxyl-terminated-polyamidoamine-grafted magnetic graphene oxide," *Materials Review*, vol. 33, pp. 234–239, 2019.

[47] S. Sobhanardakani, M. Ghoochian, S. Jameh-Bozorghi, and R. Zandipak, "Assessing of removal efficiency of indigo carmine from wastewater using MWCNTs," *Iranian Journal of Science and Technology, Transaction A- Science*, vol. 41, no. 4, article 312, pp. 1047–1053, 2017.

[48] N. M. Mahmoodi, M. Taghizadeh, and A. Taghizadeh, "Activated carbon/metal-organic framework composite as a bio-based novel green adsorbent: preparation and mathematical pollutant removal modeling," *Journal of Molecular Liquids*, vol. 277, pp. 310–322, 2019.

[49] N. M. Mahmoodi, M. Oveisi, A. Taghizadeh, and M. Taghizadeh, "Synthesis of pearl necklace-like ZIF-8@chitosan/PVA nanofiber with synergistic effect for recycling aqueous dye removal," *Carbohydrate Polymers*, vol. 227, article 115364, 2019.

[50] R. Zandipak and S. Sobhanardakani, "Synthesis of $NiFe_2O_4$-nanoparticles for removal of anionic dyes from aqueous solution," *Desalination and Water Treatment*, vol. 57, no. 24, pp. 11348–11360, 2016.

[51] S. Sobhanardakani, R. Zandipak, and R. Sahraei, "Removal of Janus Green dye from aqueous solutions using oxidized multiwalled carbon nanotubes," *Toxicological & Environmental Chemistry*, vol. 95, no. 6, pp. 909–918, 2013.

[52] S. Sobhanardakani and R. Zandipak, "Removal of anionic dyes (direct blue 106 and acid green 25) from aqueous solutions using oxidized multi-walled carbon nanotubes," *Iranian Journal of Health Sciences*, vol. 3, pp. 48–57, 2015.

[53] S. Arivoli and M. Thenkuzgali, "Kinetic, mechanistic, thermodynamic and equilibrium studies on the adsorption of rhodamine B by acid activated low cost carbon," *E-Journal of Chemistry*, vol. 5, no. 2, article 437375, pp. 187–200, 2008.

[54] N. M. Mahmoodi, M. Taghizadeh, and A. Taghizadeh, "Mesoporous activated carbons of low-cost agricultural bio-wastes with high adsorption capacity: preparation and artificial neural network modeling of dye removal from single and multicomponent (binary and ternary) systems," *Journal of Molecular Liquids*, vol. 269, pp. 217–228, 2018.

[55] N. M. Mahmoodi, B. Hayati, and M. Arami, "Textile dye removal from single and ternary systems using date stones: kinetic, isotherm, and thermodynamic studies," *Journal of Chemical & Engineering Data*, vol. 55, no. 11, pp. 4638–4649, 2010.